



Study on microstructure evolution of AISI 304 stainless steel joined by rotary friction welding

Guilong Wang^{1,2} · Jinglong Li¹ · Jiangtao Xiong¹ · Wei Zhou¹ · Fusheng Zhang¹

Received: 14 August 2017 / Accepted: 24 May 2018 / Published online: 5 June 2018
© International Institute of Welding 2018

Abstract

The object of the present work is to research the microstructure evolution of AISI 304 stainless steel (304SS) joined by rotary friction welding. The dynamic recrystallization (DRX) and texture formation process were analyzed by optical microscope and electron back-scattered diffraction (EBSD) technology. The results showed that DRX, which emerges on the torque rising stage, mainly occurs in the welding zone, and completes on the torque quasi-steady stage. Furthermore, obvious shear type texture ($\{110\} \langle 112 \rangle$) forms in the joint of 304SS.

Keywords Rotary friction welding · 304SS · DRX · Texture

1 Introduction

AISI 304 stainless steel (304SS) has been widely used as nuclear structural materials for reactor coolant piping, valve bodies, and vessel internals owing to its superior corrosion resistance properties even under high temperature and excellent low temperature toughness. 304SS is preferred over other stainless steels as the advantages in both welding and deformation [1, 2]. However, problems such as the HAZ cracking caused by the intergranular Cr-rich carbides along the grain boundaries in HAZ, coarse grains, and creep failure are often encountered in welding of 304SS by the conventional arc welding [3–5].

These negative effects can be minimized by adopting rotary friction welding (RFW) [6]. As a solid-state process, the peak temperatures involved in RFW do not exceed the melting temperature of the base material. RFW is now well established as a means of joining many different types of materials because it

has proved to be a reliable and economical way of producing high-quality welds [7, 8]. Several authors have demonstrated that RFW is suitable for the welding of 304SS [6, 9, 10].

During RFW process, steep gradient of strain, strain rate, and temperature occur in the welding joint, which result in the microstructural transformations, like dynamic recrystallization (DRX) and texture formation [8]. Lots of literatures investigated the relationship between microstructure and mechanical properties of 304SS welded by friction welding.

Sathiya et al. [11] investigated the metallurgical and mechanical properties of rotary friction welded 304SS. The correlation between the microstructure and the joint strength was also discussed. The result showed that the grain size of the joint was affected by the joining process parameters; meanwhile, the microstructure can be correlated to mechanical properties of the joint.

Yutaka et al. [12] studied the recrystallization phenomenon during friction stir welding of 304SS. The result showed that the welding zone underwent DRX. In the stir zone, a $\langle 100 \rangle$ fiber texture component containing a dominant orientation was observed from the center to the advancing side.

Kumar et al. [13] investigated the effect of texture on corrosion properties of AISI 304SS. He found that at lower cold reduction levels, when the cold rolling texture just begins to develop, electrochemical and pitting potential behavior is controlled by tensile rolling stresses. However, at higher cold reduction levels, sharp rolling texture nullifies the adverse effect of the cold rolling residual stresses, and it minimizes the deterioration of corrosion properties in the presence of tensile.

Recommended for publication by Commission III - Resistance Welding, Solid State Welding, and Allied Joining Process

✉ Guilong Wang
wanguilongnos@mail.nwpu.edu.cn

¹ Shaanxi Key Laboratory of Friction Welding Technologies, Northwestern Polytechnical University, Xi'an 710072, People's Republic of China

² Key Laboratory of Solidification Processing, Northwestern Polytechnical University, Xi'an 710072, People's Republic of China

Table 1 Nominal chemical composition of 304 stainless steel (wt%)

Element	Fe	C	Si	Mn	Cr	Ni	S	P
Content	Bal.	0.10	0.6	1.8	18	9	0.01	0.02

However, the number of reports on the details of microstructural evolution in RFW of 304SS, especially DRX and texture development process, is limited despite the importance of microstructural evolution on the mechanical properties.

The object of the present study is to examine the microstructural evolution process of 304SS during RFW. The microstructure of the joints is examined by optical microscope (OM) and electron backscatter diffraction (EBSD) to obtain the knowledge of the microstructural evolution, especially the DRX and texture development.

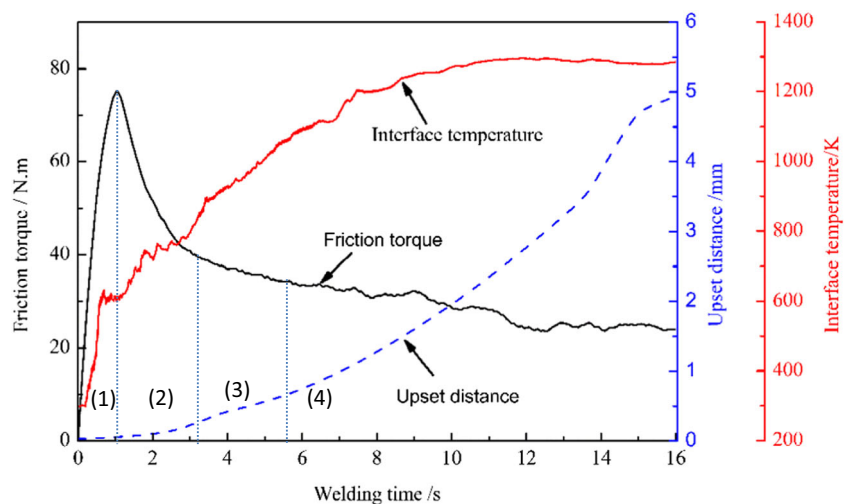
2 Experimental procedure

The material used in the present investigation was the 304SS with the nominal composition listed in Table 1. Workpieces with a diameter of 25 mm diameter were joined by RFW. The welding machine used in the RFW experiment is C320 friction welding machine. The welding parameters are shown in Table 2. The friction torque was recorded by computer through an A/D converter with sampling time of 0.01 s. The interface temperature of the joints was measured by infrared

Table 2 Welding parameters

Rotational speed (rpm)	Friction pressure and axial force (MPa) (KN)	Burn-off length (mm)	Forge pressure (MPa)	Forge time (s)
1500	80 (39.25)	2	80	6

Fig. 1 Evolution of the frictional torque, interface temperature and upset distance of the joint, and the welding stopped stage: (1) torque rising stage, (2) torque decreasing stage, (3) torque quasi-steady stage, and (4) torque steady stage



thermal imaging instrument (Tec VarioCAM@hr., head-HS Infra) with sampling time of 0.02 s. A pair of thermocouple is spot welding on the stationary side of the and close to flash region, to calibrate the data collected by infrared thermography instrument, based on the consistency of the thermocouple and infrared measurements. On this basis, the emissivity of 304SS is 0.8. Figure 1 shows a representative torque and temperature curves. To clarify the microstructure evolution process, the welding process was stopped at different stages of torque as illuminated in Fig. 1. And the joints were cooled down in water to preserve the microstructure.

The axial cross-section of the joints was obtained for microstructural examination after welding. The samples for OM examination were mounted for polishing, then etched by a reagent of 5 g FeCl_3 solved in dilute hydrochloric acid (15 ml HCl + 60 ml H_2O). The samples for EBSD examination were prepared by electrochemical polishing at 20 V in a polishing solution of 5% HClO_4 + 95% $\text{C}_2\text{H}_5\text{OH}$ for 60 s. The EBSD detector was an Oxford Nordlys X-max with analysis software of HKL Channel 5 System (Oxford Instruments) equipped in a scanning electron microscope (Tescan-VEGAILMH).

3 Results and discussion

3.1 Microstructure of the base metal

The base metal (BM) is 304SS rods of which supply state is annealing treatment after rolling. The initial microstructure consists of uniform equiaxed grains with an average size of 25 μm , as shown in Fig. 2.

Figure 3 shows the EBSD map and misorientation angle distribution of the BM. Grains are colored in terms of the crystal direction in the EBSD map (Fig. 3a). Results show that the grain orientation of BM is relatively uniform, and

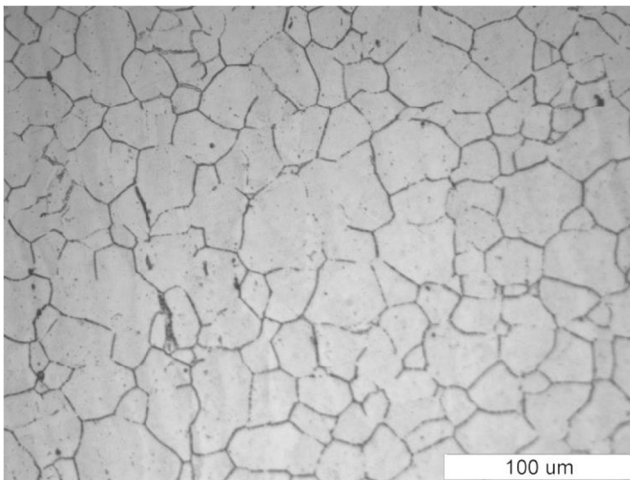


Fig. 2 Microstructure of the 304SS base metal

no special high-density orientation distribution. The statistical results of grain orientation angle are shown in Fig. 3b. It is generally believed that the grain boundary angle of high-angle boundaries (HABs) is larger than 15°, and low-angle boundaries (LABs) are less than 15°. In addition, HABs are formed after recrystallization because of the arbitrary orientation of recrystallization grains [14]. From the statistical results, it can be seen that the proportion of HABs in the BM accounted for 97.6%. It indicates that there are a large number of recrystallization grains which generated during annealing in the BM.

Fig. 3 Features of microstructure of the base material shown by a EBSD map and b misorientation distribution

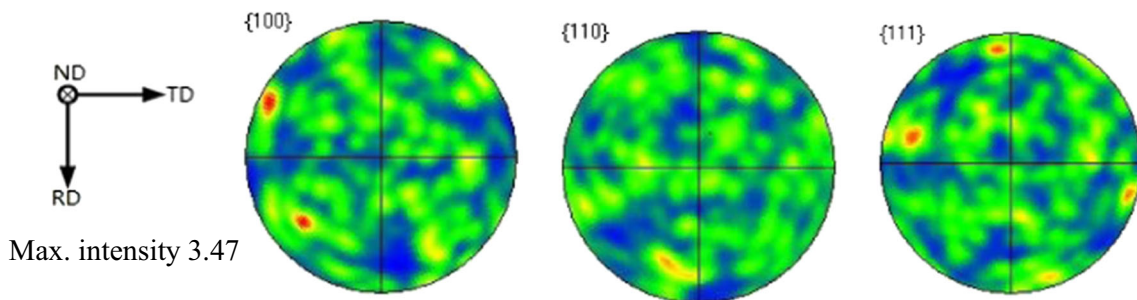
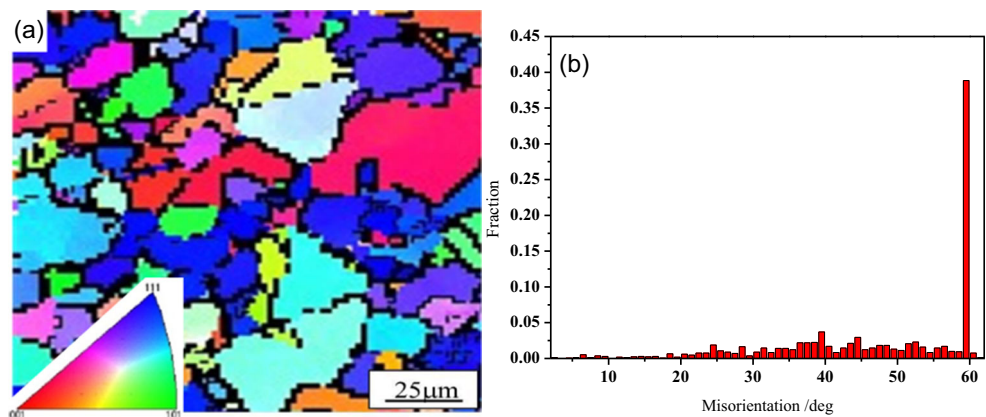


Fig. 4 {100}, {110}, and {111} pole figures of the BM

Figure 4 shows the {100}, {110}, and {111} pole figures of the BM. The RD, TD, and ND refer to the rolling direction, transverse direction, and normal direction, respectively. The maximum intensity of pole figures is 3.47 in the BM. The results further suggest that the BM exhibits a relatively random texture, i.e., no obvious micro texture in the BM.

3.2 Dynamic recrystallization evolution in the WZ

Figure 5 shows the cross-section macro morphology and microstructure morphology of welded joint. Four zones consisting of weld zone (WZ), thermo-mechanically affected zone (TMAZ), heat-affected zone (HAZ), and base metal (BZ) can be observed. The WZ consists of equiaxed grains as the reason that sufficient DRX occurs in the WZ [15]. While, TMAZ occurs partial DRX and no DRX occurs in the HAZ. Therefore, to clarify the DRX evolution during RFW process, stop the welding process at different stages, as have been illuminated in Fig. 1. The joint was cooled down in water immediately to preserve the microstructure. Then, the macrostructure and microstructure of WZ on each stage were examined by OM, as shown in Figs. 6 and 7, respectively.

During the torque rising stage, DRX occurs in the partial area of the welding interface (Fig. 6a), and the recrystallization grains are fine (Fig. 7a). On this stage, the temperature, as well as the stored energy and dislocation density in the WZ, increases with the welding process. On the welding interface, the ring area of 1/3~2/3 radius away from the axis has the

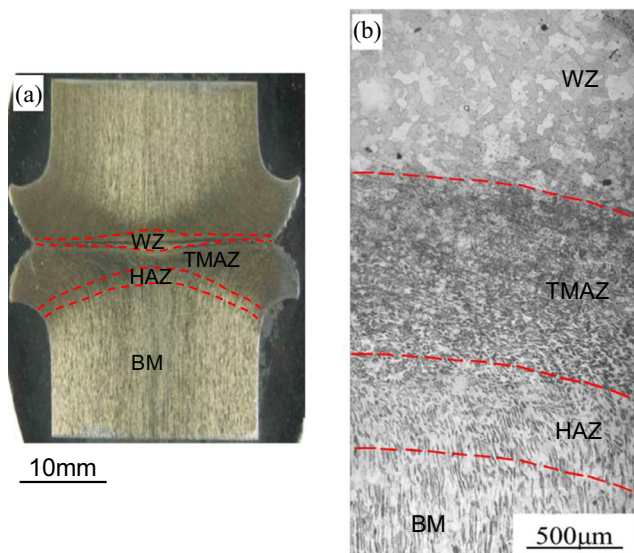
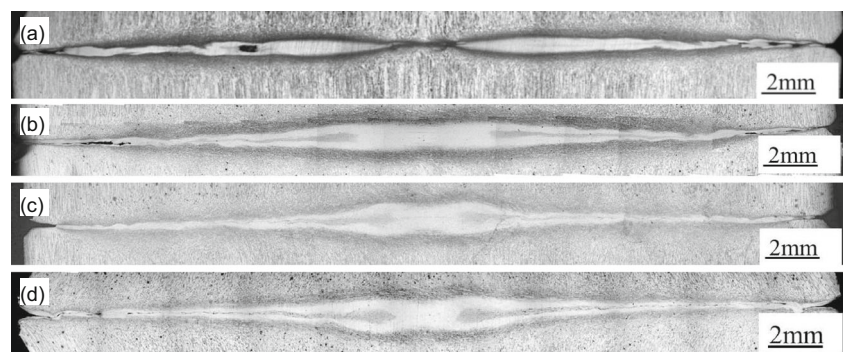


Fig. 5 Section macro morphology (a) and microstructure morphology (b) of 304SS RFW joint

highest temperature and experiences the most severe plastic deformation [16]. Therefore, the most obvious DRX occurs in this area. However, as Fig. 1 shows, since the torque rising rapidly to the peak value when the RFW process starts, the duration of torque rising stage is only about 1 s. In addition, the highest temperature of the joint during this stage is 617 K, which is not high enough for coarse grains generation. Thus, the fine recrystallization grains with an average diameter of 1.2 μm exist in the WZ.

During the torque decreasing stage, DRX occurs on the whole welding interface (Fig. 6b) and the WZ consists of equiaxed grains (Fig. 7b). It is analyzed that the dislocation density in the WZ reduces gradually with DRX process. Couple with the increasing of strain and temperature, more DRX grains form on the un-recrystallized material. The formation of new grains continuing with further deformation and eventually extends to the entire welding interface. Compare Fig. 7b with Fig. 7a, the DRX grains on torque decreasing stage are coarser than those on torque rising stage, the reason is that grains grow under the action of thermal and deformation on torque decreasing stage.

Fig. 6 Evolution of macrostructure of the WZ. **a** Torque rising stage. **b** Torque decreasing stage. **c** Torque quasi-steady stage. **d** Torque steady stage



During the torque quasi-steady stage, the joint is completely bonding, as shown in Fig. 6c. The WZ consists of equiaxed grains which turn coarser compare with those on torque decreasing stage. With the welding process, the heat produced by friction and plastic deformation further increase. Meanwhile, the temperature and the deformation tend to be uniform on the friction interface. Under the effect of high temperature, as well as severe plastic deformation and axial pressure, adequate DRX occurs in the WZ. Simultaneously, DRX grains further grow due to the increasing of temperature, as shown in Fig. 7c.

During the torque steady stage, there is no obvious change in the morphology of the WZ compare with that on torque quasi-steady stage. The grains with an average diameter of 18 μm exist in the WZ, which nearly equal to that of the BM (25 μm). It is analyzed that the heat generation and dissipation reach a balance on this stage; thus, the joint nearly keeps at a stable temperature, as shown in Fig. 1. In addition, the work hardening phenomenon that corresponds to dislocation proliferation and DRX process that corresponds to dislocation disappearance also reaches a balance. Thus, the macrostructure of the WZ has no obvious change. However, with the time increasing, the size of DRX grains increases due to the heat accumulation and finally, the microstructure is replaced by relatively equiaxed grains with an average grain size of 18 μm .

3.3 EBSD analysis of microstructure evolution in the weld zone

According to the above analysis, DRX emerges on torque rising stage in the WZ and completes on torque quasi-steady stage. Thus, the characteristics of the microstructure of the WZ on these two stages were studied by EBSD technology to further investigate the DRX evolution behavior and grains orientation during RFW.

Figure 8 shows the EBSD map and misorientation angle distribution in the WZ on torque rising stage. As it is seen, green dominates in the EBSD map, which indicates that the grain orientation mainly concentrates in the normal direction of crystallographic plane $\{110\}$. The statistical result of grain orientation angle indicates that the proportion of LABs is 30%. It obviously

Fig. 7 Evolutions of microstructure of the WZ. **a** Torque rising stage. **b** Torque decreasing stage. **c** Torque quasi-steady stage. **d** Torque steady stage

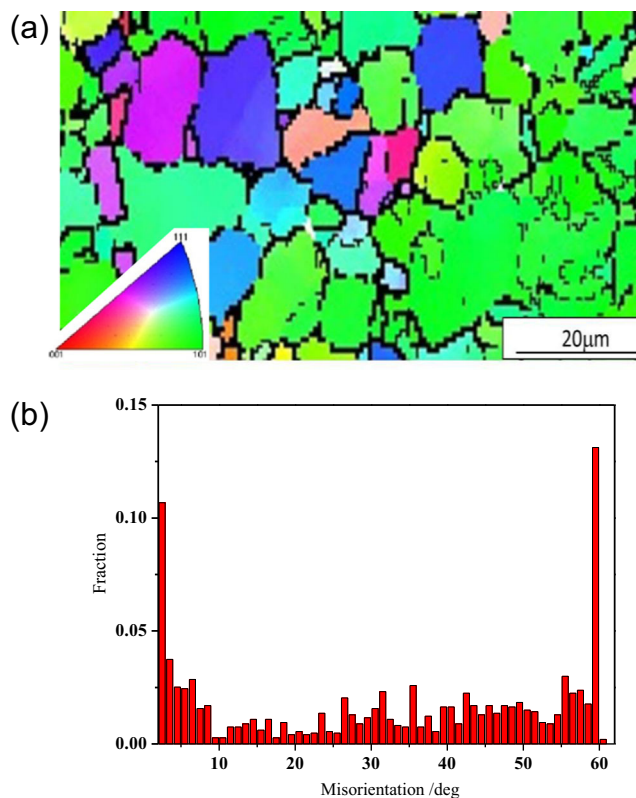
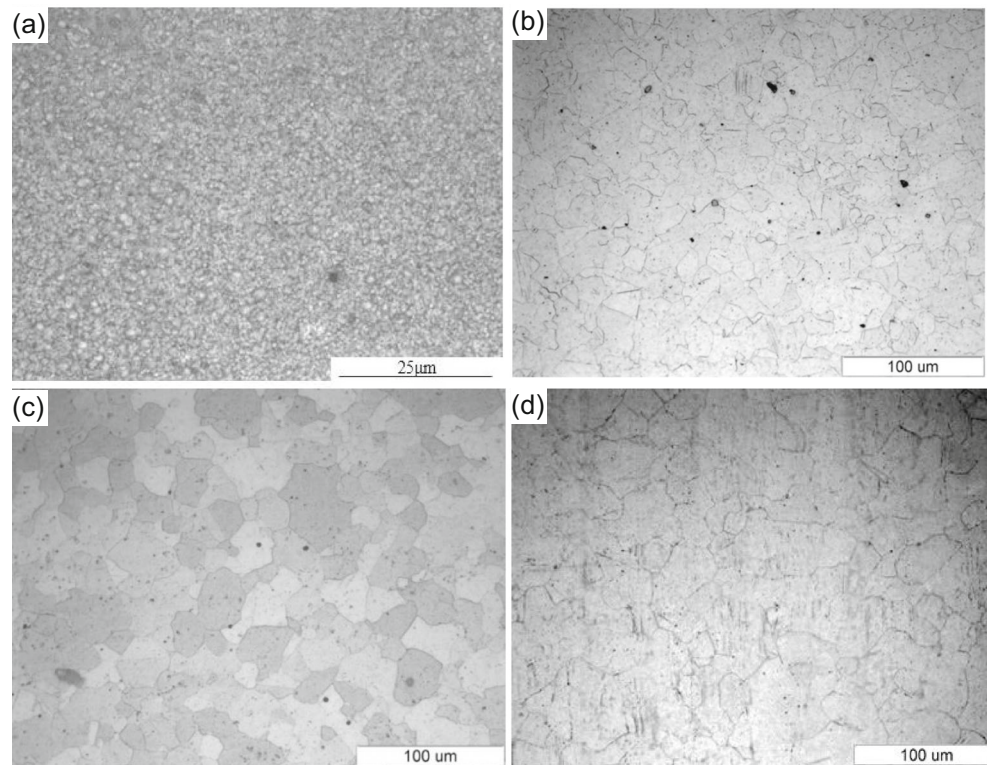


Fig. 8 Microstructure characteristic of the WZ on torque rising stage shown by **a** EBSD map and **b** misorientation distribution

increases compared with that of the BM (3.4%). On the other hand, the proportion of HABs decreases to 70%. The reason is that, the original grains in the BM are segmented into a number of cellular substructures due to the slipping and the pile-up of dislocation on torque rising stage. This phenomenon results in decreasing of the HABs. Above analysis further indicates that DRX occurs in the WZ during this stage.

Figure 9 shows the $\{100\}$, $\{110\}$, and $\{111\}$ pole figures of the WZ on torque rising stage. The maximum intensity of pole figures is 10.57, which is an obvious increase compared with that of the BM (3.47). It proves that the texture is formed in the WZ, of which the $\{111\}$ crystallographic plane parallels to the welding surface, and the $\langle 110 \rangle$ crystal direction parallels to the frictional direction (the shear direction). Since the face-centered-cubic structure, the slip system of 304SS is $\{111\} \langle 110 \rangle$. And the sub grains are formed due to the dislocation-tangle. Meanwhile, the sub grains rotate under the action of axial pressure and torsional loading that result in the activation of the slip system. The slip surface $\{111\}$ rotates around the vertical direction of the workpiece's axial (i.e., RD direction), and the normal direction of the slip surface is coincident with the axial pressure direction. Thus, the $\{111\}$ crystallographic planes and $\langle 110 \rangle$ crystal direction of the grains in the WZ parallel to the welding surface and frictional direction, respectively.

Figure 10 shows the EBSD map and misorientation angle distribution of the WZ on the torque quasi-steady stage. The blue color dominated in the EBSD map which indicates that

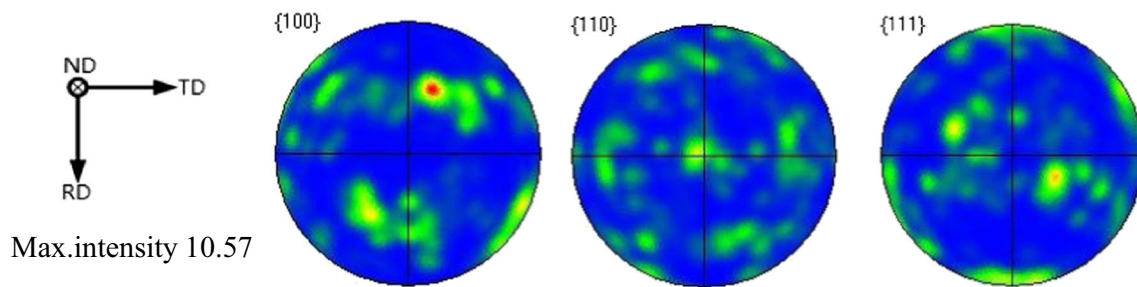


Fig. 9 $\{100\}$, $\{110\}$, and $\{111\}$ pole figures of the WZ on torque rising stage

the grain orientation is mainly concentrated in the normal direction of $\{111\}$ crystallographic plane. The statistical results of grain orientation angle in the WZ indicate that the proportion of HABs is 77%, which increases compare with that on the torque rising stage (70%). While the LABs' proportion decrease to 23%. The reason is that the temperature of the WZ increase with the welding process on this stage results in the dislocation moving easily. Meanwhile, with the increasing of deformation in the WZ, the dislocation wall that is perpendicular to the slipping surface is formed by the dislocation pile-up. Then, the dislocation wall further develops to the sub grains. Because the attraction effect between stress field and dislocation, the unstable sub grain boundary absorb the moving dislocations in grains. This leads to the increasing of

orientation difference of grain boundary. Eventually, the sub grain boundaries transform into HABs.

Figure 11 shows the $\{100\}$, $\{110\}$, and $\{111\}$ pole figures of WZ on torque quasi-steady stage. The maximum intensity of pole figures is 6.2. As it is seen, the $\{110\}$ crystallographic plane parallels to the welding surface, and the $\langle 111 \rangle$ crystal direction parallels to the TD direction. Thus, the $\langle 112 \rangle$ crystal direction parallels to the ND direction. According to the former research [17], 304SS mainly has the brass type texture ($\{110\} \langle 112 \rangle$) when it subject to large shear stress. Since the WZ undergoes the axial pressure and shear stress along the normal direction during RFW, obvious shear type texture ($\{110\} \langle 112 \rangle$) eventually forms in the joint of 304SS welded by RFW.

Fig. 10 Characteristic microstructure of the WZ on torque quasi-steady stage shown by **a** EBSD map and **b** misorientation distribution

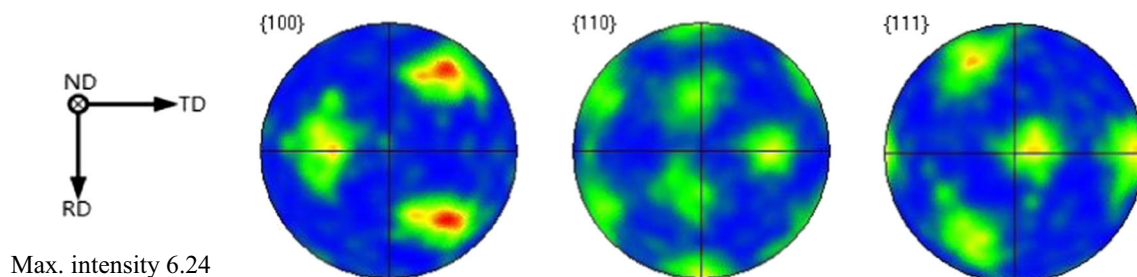
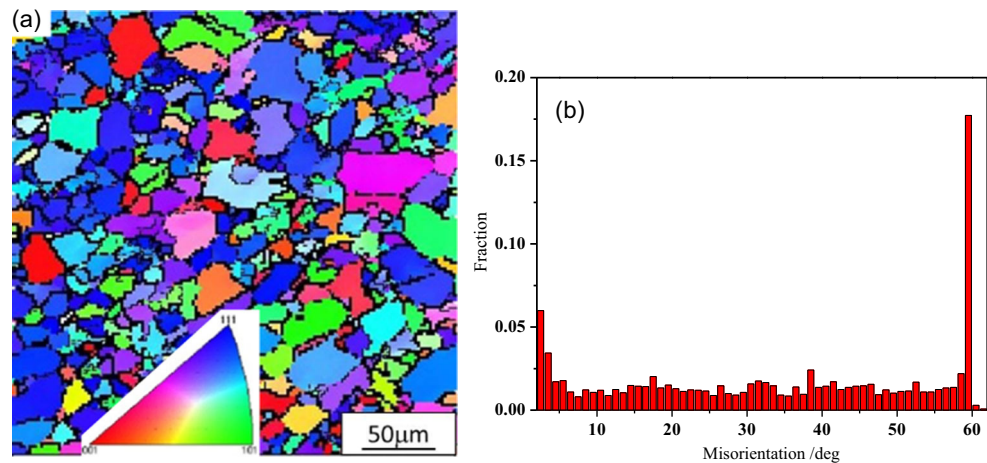


Fig. 11 $\{100\}$, $\{110\}$, and $\{111\}$ pole figures of the WZ on torque quasi-steady stage

4 Conclusion

The microstructure characteristics of 304SS joint welded by RFW were studied. The conclusions are as follows:

- (1) DRX emerges in the torque rising stage in WZ and completes on the torque quasi-steady stage. On the torque rising stage, the recrystallization grains with an average diameter of 1.2 μm exist in the WZ. The grains gradually grow up with the welding process. Eventually, the average diameter of WZ is 18 μm , which nearly equal to that of the BM (25 μm).
- (2) The proportion of LABs in WZ is 30% on torque rising stage, which was significantly higher than that of BM (3.4%). With the welding process, the moving dislocations are absorbed by the sub grain boundaries, which gradually transform into HABs. Finally, the proportion of LABs in WZ is 23%.
- (3) EBSD pole figures show that there is no obvious micro texture in the BM. During torque rising stage, metal in the WZ starts to slip under the action of axial pressure. The slip surface $\{111\}$ rotates to the direction that parallels to the welding surface. The $\langle 110 \rangle$ crystal direction parallels to the frictional direction. Eventually, obvious shear texture ($\{110\} \langle 112 \rangle$) appears in the WZ with the welding process.

Funding information This work was supported by the National Natural Science Foundation of China (Grand No.: 51475376, 51575451).

References

1. Tavares SSM, Fruchart D, Miraglia S (2000) A magnetic study of the reversion of martensite α' in a 304 stainless steel. *J Alloys Compd* 307(1):311–317
2. Sahin M (2009) Characterization of properties in plastically deformed austenitic-stainless steels joined by friction welding. *Mater Des* 30(1):135–144
3. Lima AS, Nascimento AM, Abreu HFG, de Lima-Neto P (2005) Sensitization evaluation of the austenitic stainless steel AISI 304L, 316L, 321 and 347. *J Mater Sci* 40(1):139–144
4. Yan J, Gao M, Zeng X (2010) Study on microstructure and mechanical properties of 304 stainless steel joints by TIG, laser and laser-TIG hybrid welding. *Opt Lasers Eng* 48(4):512–517
5. Kumar S, Shahi AS (2011) Effect of heat input on the microstructure and mechanical properties of gas tungsten arc welded AISI 304 stainless steel joints. *Mater Des* 32(6):3617–3623
6. Sathiya P, Aravindan S, Haq AN (2008) Some experimental investigations on friction welded stainless steel joints. *Mater Des* 29(6):1099–1109
7. Kimura M, Inoue H, Kusaka M et al (2010) Analysis method of friction torque and weld interface temperature during friction process of steel friction welding. *J Solid Mech Mater Eng* 4(3):401–413
8. Uday MB, Ahmad Fauzi MN, Zuhailawati H, Ismail AB (2010) Advances in friction welding process: a review. *Sci Technol Weld Join* 15(7):534–558
9. Sahin M (2007) Evaluation of the joint-interface properties of austenitic-stainless steels (AISI 304) joined by friction welding. *Mater Des* 28(7):2244–2250
10. Umanath K, Palanikumar K (2015) Influence of process parameter on microstructural characteristics and tensile properties of friction welded ASS304L alloy. *Appl Mech Mater* 766-767:745–750
11. Sathiya P, Aravindan S, Haq AN (2005) Mechanical and metallurgical properties of friction welded AISI 304 austenitic stainless steel. *Int J Adv Manuf Technol* 26(5–6):505–511
12. Sato YS, Nelson TW, Sterling CJ (2005) Recrystallization in type 304L stainless steel during friction stirring. *Acta Mater* 53(3):637–645
13. Kumar BR, Singh R, Mahato B et al (2005) Effect of texture on corrosion behavior of AISI 304L stainless steel. *Mater Charact* 54(2):141–147
14. Wu GL, Godfrey A, Jensen DJ, Liu Q (2005) Deformation strain inhomogeneity in columnar grain nickel. *Scr Mater* 53(5):565–570
15. Zhu Y, Zhu Z, Xiang Z, Yin Z, Wu Z, Yan W (2009) Microstructural evolution in 4Cr 10 Si 2 Mo at the 4Cr 10 Si 2 Mo/Nimonic 80A weld joint by inertia friction welding. *J Alloys Compd* 476(1):341–347
16. Kimura M, Kusaka M (2003) Observation of joining phenomena in friction stage and improving friction welding method. *JSME International Journal Series A Solid Mechanics and Material Engineering* 46(3):384–390
17. Leffers T, Ray RK (2009) The brass-type texture and its deviation from the copper-type texture. *Prog Mater Sci* 54(3):351–396